Steel and Composite Structures, *Vol. 34, No. 2 (2020) 227-239*
DOI: https://doi.org/10.12989/scs.2020.34.2.227

Nonlinear and post-buckling responses of FGM plates with oblique elliptical cutouts using plate assembly technique

S.A.M. Ghannadpour* and M. Mehrparvar

New Technologies and Engineering Department, Shahid Beheshti University, G.C, Tehran, Iran

(*Received August 12, 2019, Revised November 21, 2019, Accepted November 27, 2019*)

Abstract. The aim of this study is to obtain the nonlinear and post-buckling responses of relatively thick functionally graded plates with oblique elliptical cutouts using a new semi-analytical approach. To model the oblique elliptical hole in a FGM plate, six plate-elements are used and the connection between these elements is provided by the well-known Penalty method. Therefore, the semi-analytical technique used in this paper is known as the plate assembly technique. In order to take into account for functionality of the material in a perforated plate, the volume fraction of the material constituents follows a simple power law distribution. Since the FGM perforated plates are relatively thick in this research, the structural model is assumed to be the first order shear deformation theory and Von-Karman's assumptions are used to incorporate geometric nonlinearity. The equilibrium equations for FGM plates containing elliptical holes are obtained by the principle of minimum of total potential energy. The obtained nonlinear equilibrium equations are solved numerically using the quadratic extrapolation technique. Various sets of boundary conditions for FGM plates and different cutout sizes and orientations are assumed here and their effects on nonlinear response of plates under compressive loads are examined.

Keywords: post-buckling behavior; oblique elliptical cutouts; functionally graded plates; plate assembly technique; penalty method, Mapping

1. Introduction

In the past few years, functionally graded materials (FGMs) which were introduced by a group of material scientists in Japan in 1984 (Koizumi 1997), have received considerable attention as shielding materials for airplanes, space shuttles and other engineering applications. FGMs are microscopically inhomogeneous composites and their mechanical properties vary smoothly from a surface to another. FGMs are classically a mixture of ceramic and metal, although they could be combination of other materials as well, e.g., a mixture of different metals. The mixture of ceramic and metal displays some remarkable mechanical properties such as high fracture toughness and high degree of temperature resistance by maintaining the desired structural integrity.

Cutouts are often found in plate structures due to weight optimization, ventilation, access for hardware, electric lines and fuel lines to pass through and in case of fuselage windows and doors. However, the plate's stability may get compromised due to presence of hole and the membrane stresses may rearrange in the plates. Therefore, studying the buckling of perforated plate is required. Some of the works in this field are presented below.

Javaheri and Eslami (2002) studied buckling of functionally graded plates under in-plane compressive load, Ghannadpour, Ovesy and Nassirnia (2012) investigated buckling behavior of functionally graded plates (FGPs) by using finite strip method and buckling of FGPs under mechanical loading has been analyzed by Sherafat, Ovesy and Ghannadpour (2013) with implement of higher-order functionally graded strip. Moreover, Britt (1994) investigated shear and compression buckling of anisotropic panels with elliptical holes. Ghannadpour *et al*. (2006) studied buckling behavior of composite plates with circular and elliptical cutouts and the effect of elliptical cutout on the buckling load of orthotropic plate has been investigated by Choudhary and Jana (2018). In addition to above studies, many other works has been done on buckling behavior of perforated plates, for instance, Baba and Baltaci (2007), Kumar and Sonmez (2008), Kumar *et al.* (2010), Cheng and Li (2012), Rajanna *et al*. (2016), Taheri-Behrooz and Omidi (2018) and Heidari-Rarani and Kharratzadeh (2019).

Alternatively, plates may sustain additional loads even after buckling happens and hence the post-buckling behavior of such plates has received many attentions. In such studies, the bifurcation load given by linear buckling analysis may not represent the carrying capability of a plate accurately. Many works have been done in this field of study, Ghannadpour and Alinia (2006) analyzed large deflection of FGPs under pressure loads, Yang and Shen (2003) studied nonlinear behavior of FGPs under transverse and in-plane loads and Ovesy and Ghannadpour (2007) used finite strip method to analyze FGPs under pressure loads. Also, more on this topic, Ma and Wang (2003), Yang *et al.* (2006), Wu *et al.* (2007), Alinia and Ghannadpour (2009), Lee *et al*. (2010), Ovesy *et al.* (2015), Kar and

*Corresponding author, Ph.D.
E-mail: a_ghannadpour@sbu.ac.ir

ISSN: 1229-9367 (Print), 1598-6233 (Online)

Panda (2016), Ma *et al*. (2018) and Ghannadpour and Kiani (2018). On the case of post-buckling behavior of perforated plates many investigations has been done, for example Nemeth (1990) worked experimentally on buckling and post-buckling behavior of plates with circular cutouts under compression, Vandenbrink and Kamat (1987) studied the response of plates with circular holes, Mohammadi *et al.* (2006) worked on effective widths of perforated cross-ply laminate under compression, Jain and Kumar (2004) investigated the post-buckling response of composite plate with circular/elliptical holes which are located at center of it. Kong *et al*. (2001) calculated post-buckling strength of composite laminate with hole and also Kumar and Singh (2010) done the same study on plates under in-plane shear with different shapes of cutout.

Many studies, involving thermal stress, vibration, buckling, static and dynamic analyses of such structures have been carried out to date, for instance Pardhan and Chakraverty (2015) done static analysis of FGPs with various boundary supports, Kandasamya *et al.* (2016) numerically studied free vibration and thermal buckling behavior of moderately thick functionally graded structures under thermal loadings and Chen *et al*. (2014) used Chebyshev–Lagrangian method to study flexural and in-plane vibration analysis of elastically restrained thin rectangular plate. Large amplitude flexural vibration of perforated laminate has been worked on by Reddy (1982), stability of laminate with cutouts by Srivatsa *et al.* (1992) and stability of panels with various cutout geometries by Bailey and Wood (1996). Noor and Kim (1996) studied buckling and post-buckling of panels which are under combined edge shear and thermal loadings and Kumar and Singh (2010) investigated the effect of boundary conditions on buckling and post-buckling behavior of laminate with different geometry of cutouts. Recently, other works has been done in the field of post-buckling and nonlinear behavior of perforated plates, for instance, Ghannadpour and Mehrparvar (2018) developed a new method to investigate the post-buckling behavior of composite plates which contain circular/ elliptical cutouts. In the mentioned method, which was called energy effect removal technique, the total potential energy of the perforated plate is obtained by subtracting the potential energy of cutout from the potential energy of a perfect plate. Also, in another study, they investigated the nonlinear behavior of functionally graded plates containing rectangular cutouts (Mehrparvar and Ghannadpour 2018). In their analysis, the perforated plates were modeled by assembling eight elements and the connections between them were provided by the Penalty method. This technique was called plate assembly technique in their paper.

In the current paper, nonlinear and post-buckling behaviors of perforated functionally graded plates has been investigated under in-plane compressive loads. This study has been conducted on FGM plates containing oblique elliptical cutout. The analysis method is based on the plate assembly technique, in which six plate-elements with both straight and curved boundaries are used for modeling the elliptic hole. To enforce the connectivity conditions between the plate-elements, the well-known Penalty method is used in this research. The structural formulation is based on the first order shear deformation theory (FSDT) and Von-Karman's assumptions. The mechanical properties of FG plates, except the Poisson's ratio, are assumed to vary continuously through the thickness of the plate, and obey a simple power law distribution in terms of the volume fractions of constituents. The fundamental equations of perforated FG plates are obtained by applying the principle of minimum of total potential energy. Since the geometric nonlinearity considerations are included in the analysis, the final system of governing equations has a nonlinear form. To solve this nonlinear set of equations, the iterative quadratic extrapolation technique is employed. Finally, the effects of cutout sizes and locations for FG plates with various sets of boundary conditions under uniaxial in-plane compressive loads are extensively determined and discussed. To investigate the accuracy of the present work, some results have been obtained by finite element analyses using ABAQUS program wherever possible.

2. Theory and formulation

A typical square plate of dimensions $l \times l$ and total thickness h which contains oblique elliptic cutout shape is shown in Fig. 1. The shape parameters a and b are called the double semi-major and double semi-minor axes, respectively. The functionally graded plate is subjected to in-plane compressive load N_x in the x-direction on vertical edges $x = \pm l/2$.

Given the fact that the FG plates in this study are relatively thick, the first order shear deformation theory is used. Describing the boundary conditions specifically is a necessity with the aim of approximating the displacement functions of the problem. Three different sets of boundary conditions are chosen here which are represented in Fig. 2. As shown in this figure, for all sets of boundary conditions, uniform movement in x-direction is allowed at edges 1 and 2 but edges 3 and 4 can move freely in y-direction for all sets of boundary conditions.

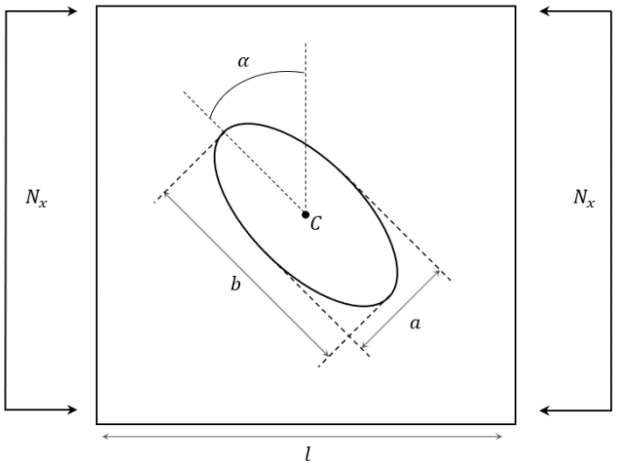

Fig. 1 A typical square plate with elliptical cutout

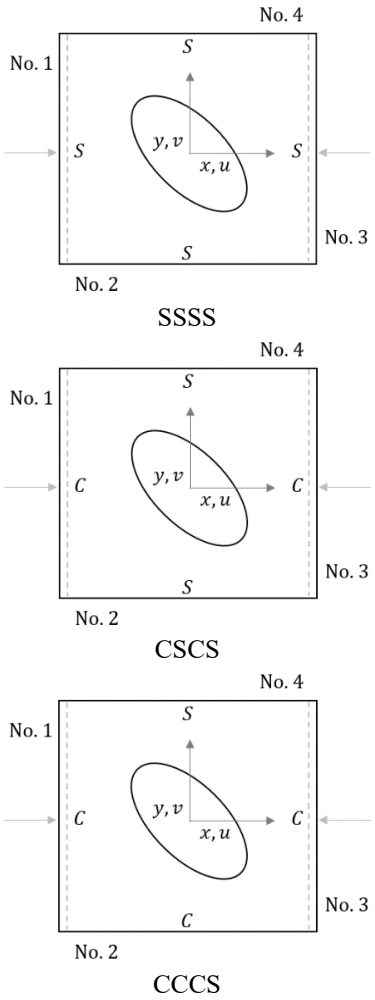

Fig. 2 Three different sets of boundary conditions

Though, as it is observed, there are some symbols and numbers in Fig. 2 to illustrate the boundary condition of each edge and edge number, respectively. For more information on these symptoms, refer to the studied done by Mehrparvar and Ghannadpour (2018), Ghannadpour and Shakeri (2018). The details of edges conditions for SSSS, CSCS and CCCS sets are expressed in Table 1. The edges number $\beta = 1,2,3,4$ that will be used later in the estimation of displacement fields is also presented in this table.

In Table 1, the phrases Free, Straight and Held mean that the edges are free to move, they can move straightly and they are held against any movement, respectively.

The perforated FG plate in this study is modeled by six plate-elements which are connected together, as shown in Fig. 3. As it can be observed, the isoperimetric mapping method can be used for elements 1, 2, 5 and 6, which are quadrilaterals with straight sides, and the same method can be used for the elements 3 and 4, which are quadrilaterals with curve sides. Here, the first step is to derive methods for quadrilateral domains with curved sides. The approach most commonly used is to create a transformation from the domain on which the solution is needed, which is called physical domain, to the square, which is called computational domain. This technique which is capable of creating an appropriate transformation between the physical and computational domains is called transfinite interpolation technique (Kopriva 2009).

This transformation is created by the linear interpolation between the four curves that represent the physical boundary in two steps. At first, mapping from the unit square to the physical domain is developed, and then incorporate the related transformation to the reference square. The transfinite mapping between the unit square and the physical domain can be written as function below (Kopriva 2009)

$$\begin{aligned} X(\bar{\xi},\bar{\eta}) = {} & (1-\bar{\xi})\Gamma_4(\bar{\eta}) + \bar{\xi}\Gamma_2(\bar{\eta}) + (1-\bar{\eta})\Gamma_1(\bar{\xi}) \\ & + \bar{\eta}\Gamma_3(\bar{\xi}) \\ & - (1-\bar{\xi})\{(1-\bar{\eta})\Gamma_1(0) + \bar{\eta}\Gamma_3(0)\} \\ & - \bar{\xi}\{(1-\bar{\eta})\Gamma_1(1) + \bar{\eta}\Gamma_3(1)\} \end{aligned} \quad (1)$$

The final mapping function is obtained when the affine transformation, i.e., $\bar{\xi} = \frac{\xi+1}{2}$ and $\bar{\eta} = \frac{\eta+1}{2}$, are applied from the unit to the reference square (Kopriva 2009).

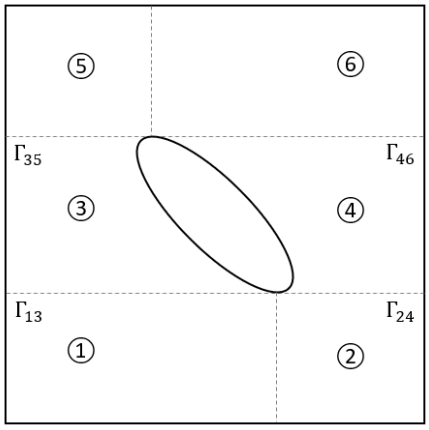

Fig. 3 Plate assembly and implementation of penalty method

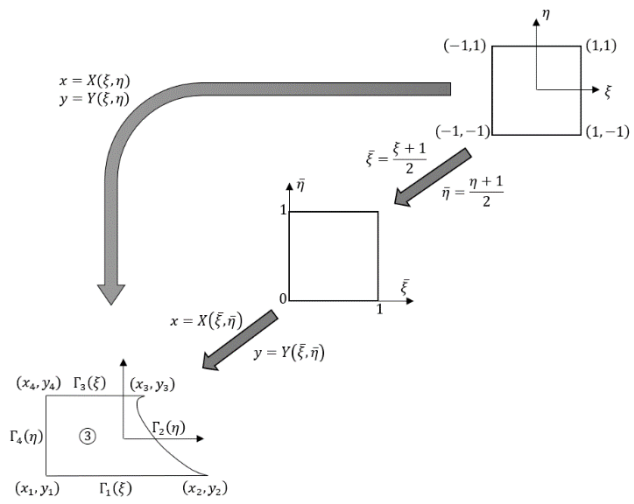

Fig. 4 Isoperimetric mapping method

Table 1 Details of edges conditions for SSSS, CSCS and CCCS

Displacement fields	Edge boundary condition											
	SSSS				CSCS				CCCS			
	1	2	3	4	1	2	3	4	1	2	3	4
u	Straight		Free		Straight		Free		Straight		Free	
v	Held				Held				Held			
w	Held											
φ_x	Free		Held									
φ_y	Held		Free		Held		Free		Held		Free	

$$
\begin{aligned}
X(\xi,\eta) = \frac{1}{2}[&(1-\xi)\Gamma_4(\eta) + (1+\xi)\Gamma_2(\eta) + (1-\eta)\Gamma_1(\xi) \\
&+ (1+\eta)\Gamma_3(\xi)] \\
&- \frac{1}{4}[(1-\xi)\{(1-\eta)\Gamma_1(-1) \\
&+ (1+\eta)\Gamma_3(-1)\} \\
&- (1+\xi)\{(1-\eta)\Gamma_1(1) + (1+\eta)\Gamma_3(1)\}]
\end{aligned} \tag{2}
$$

Finally, the transfinite mapping represented in Fig. 4, is constructed by taking the four curves and the location in computational space as input and returns it to the corresponding location in physical space, as presented by Eq. (2). Under mappings, all functions and equations are transformed, basically by result of the chain rule (Eq. (3)).

$$
\begin{aligned}
\frac{\partial \tau}{\partial x} &= \frac{\partial \tau}{\partial \xi}\frac{\partial \xi}{\partial x} + \frac{\partial \tau}{\partial \eta}\frac{\partial \eta}{\partial x} \\
\frac{\partial \tau}{\partial y} &= \frac{\partial \tau}{\partial \xi}\frac{\partial \xi}{\partial y} + \frac{\partial \tau}{\partial \eta}\frac{\partial \eta}{\partial y}
\end{aligned} \tag{3}
$$

The transformation of the derivatives can be written in matrix-vector form

$$
\begin{Bmatrix} \frac{\partial \tau}{\partial x} \\ \frac{\partial \tau}{\partial y} \end{Bmatrix} = \frac{\partial(\xi,\eta)}{\partial(X,Y)} \begin{Bmatrix} \frac{\partial \tau}{\partial \xi} \\ \frac{\partial \tau}{\partial \eta} \end{Bmatrix} \tag{4}
$$

In the above equations, parameter τ is a typical displacement component of the plate. As mentioned before, in the present study, the perforated functionally graded plate is modeled by assembly of six plate-elements and this can be shown in the formulation by the superscript i associated with the i^{th} element, as shown in Fig. 3. Each element has its own corresponding local coordinate system $x^{(i)}, y^{(i)}$ and by approximating the displacement fields with appropriate boundary conditions, it behaves as a separate plate with governing equations provided later. For the edges shared between adjoining elements, as the displacements are unknown, free boundary conditions are firstly assumed in the Ritz approximation with the purpose to recover the actual kinematics by enforcing the continuity of displacements using Penalty technique (Ghannadpour and Karimi (2018). The displacement continuity conditions along the edge Γ_{mn} can be written as

$$
\tau^{(m)}\left(x_{mn}^{(m)}, y_{mn}^{(m)}\right) = \tau^{(n)}\left(x_{mn}^{(n)}, y_{mn}^{(n)}\right) \tag{5}
$$

where $\tau^{(i)} \in \left\{u_0^{(i)}, v_0^{(i)}, w_0^{(i)}, \varphi_x^{(i)}, \varphi_y^{(i)}\right\}$ is the displacement component correspond to the mid-plane of the i^{th} element and $\left(x_{mn}^{(m)}, y_{mn}^{(m)}\right)$ and $\left(x_{mn}^{(n)}, y_{mn}^{(n)}\right)$ are the local coordinates describing the shared edge, Γ_{mn}, between $\Omega^{(m)}$ and $\Omega^{(n)}$, respectively.

Because in this research the plate assembly technique is used, therefore, for the modeling of the whole plate containing the cut-out, after establishing the connection conditions of the plate-elements, the total potential energy of all the elements $\Pi^{(i)}$must be combined together. The total potential energy of the whole plate Π can be simply obtained by summation of the total potential energy of plate-elements $\Pi^{(i)}$and penalty terms associated with the appropriate constraints.

$$
\Pi = \sum_{i=1}^{6} \Pi^{(i)} + P \tag{6}
$$

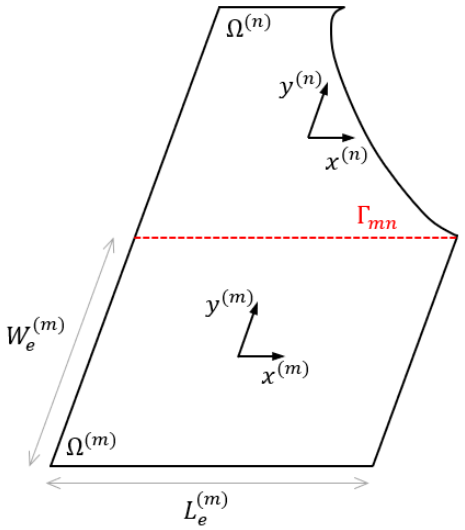

Fig. 5 Geometry configuration of shared edge between n^{th} and m^{th} elements

The penalty terms presented in Eq. (6) with respect to Fig. 5, can be written as

$$P = \sum P_{\alpha\beta}^{\langle m,n\rangle} = \sum \frac{\omega_{m,n}^{\langle\tau\rangle}}{2} \int_{\Gamma_{mn}} \left(\tau^{(m)}\left(x_{mn}^{(m)}, y_{mn}^{(m)}\right) - \tau^{(n)}\left(x_{mn}^{(n)}, y_{mn}^{(n)}\right)\right)^2 d\Gamma, \quad \alpha,\beta = m,n \tag{7}$$

and ω_{mn} is a diagonal matrix of penalty coefficients (Ghannadpour *et al.* 2019).

From here on, for the calculation of the potential energy of the plate-elements, it is necessary to define the displacements of the plates. The displacement fields for each plate-element, which are based on the first-order shear deformation plate theory (Reddy 2004) and Von-Karman assumptions, can be expressed in the form of

$$\begin{aligned} u^{(i)}(x,y,z) &= u_0^{(i)}(x,y) + z\varphi_x^{(i)}(x,y) \\ v^{(i)}(x,y,z) &= v_0^{(i)}(x,y) + z\varphi_y^{(i)}(x,y) \\ w^{(i)}(x,y,z) &= w_0^{(i)}(x,y) \end{aligned} \tag{8}$$

where $u_0^{(i)}$, $v_0^{(i)}$, $w_0^{(i)}$, $\varphi_x^{(i)}$ and $\varphi_y^{(i)}$ are unknown functions to be approximated. Parameters $u_0^{(i)}$, $v_0^{(i)}$ and $w_0^{(i)}$ are displacements of mid-surface and $\varphi_x^{(i)}$ and $\varphi_y^{(i)}$ denote the rotations of a transverse normal about axes parallel to the η and ξ axes, respectively. Meanwhile, the Rayleigh–Ritz technique is used in this study to approximate the displacement fields which have to satisfy only the aforementioned essential boundary conditions. The approximation of displacement fields is performed by Legendre polynomials $P_n(x)$ (Ghannadpour and Shakeri 2018).

Therefore, the displacement fields of the mid-surface can be approximated by following relations.

$$\tau^{(i)}\left(x^{(i)}, y^{(i)}\right) = \mathbb{B}_\tau^{(i)}\left(x^{(i)}, y^{(i)}\right) \sum_{n=1}^{N_t}\sum_{m=1}^{N_t} \delta_{mn}^{\tau^{(i)}} P_{m-1}\left(\frac{2x^{(i)}}{L_e^{(i)}}\right) P_{n-1}\left(\frac{2y^{(i)}}{W_e^{(i)}}\right) + f_\tau^{(i)}\left(x^{(i)}, y^{(i)}\right)\delta_c^{\tau^{(i)}}, \quad i = 1,\dots,6 \tag{9}$$

where the parameters $L_e^{(i)}$ and $W_e^{(i)}$ are length and width of each element, respectively and N_t is the number of terms in series expansion which is taken same for all displacement fields. The coefficients $\delta_{mn}^{\tau^{(i)}}$ and $\delta_c^{\tau^{(i)}}$ are the Ritz unknown coefficients of the problem for each element and the latter is for satisfying the straight conditions for in-plane displacement u which means that the edge is allowed to move longitudinally but is kept straight. Therefore, the boundary function $f_\tau^{(i)}(x,y)$ is also selected to guarantee the satisfaction of the straight boundary conditions at the loaded edges of the plates as mentioned in Fig. 2 (Mehrparvar and Ghannadpour 2018). The function $\mathbb{B}_\tau^{(i)}$, called boundary condition function here, also chosen to ensure the fulfillment of the essential boundary conditions mentioned in Table 1, which can be defined as

$$\mathbb{B}_\tau^{(i)}\left(x^{(i)}, y^{(i)}\right) = \prod_{\beta=1,3}\left(1 + (-1)^{\beta-1}\frac{2x^{(i)}}{L_e^{(i)}}\right)^{\mu_\beta^{\tau^{(i)}}} \prod_{\beta=2,4}\left(1 + (-1)^{\beta-1}\frac{2y^{(i)}}{W_e^{(i)}}\right)^{\mu_\beta^{\tau^{(i)}}} \tag{10}$$

Where the exponents $\mu_\beta^{\tau^{(i)}}$ can take value 0 for free condition and value 1 according to the conditions of held or straight for each displacement field $\tau^{(i)} \in \left\{u_0^{(i)}, v_0^{(i)}, w_0^{(i)}, \varphi_x^{(i)}, \varphi_y^{(i)}\right\}$.

According to von-Karman nonlinear strain–displacement relations, the strains can be expressed as follow

$$\varepsilon_s^{(i)} = \begin{bmatrix} \varphi_y^{(i)} + \dfrac{\partial w_0^{(i)}}{\partial y} \\ \varphi_x^{(i)} + \dfrac{\partial w_0^{(i)}}{\partial x} \end{bmatrix}$$

$$\varepsilon^{(i)} = \begin{Bmatrix} \varepsilon_{xx}^{(i)} \\ \varepsilon_{yy}^{(i)} \\ \varepsilon_{xy}^{(i)} \end{Bmatrix} = \varepsilon^{0(i)} + z\psi^{(i)}; \tag{11}$$

$$\varepsilon^{0(i)} = \begin{Bmatrix} \varepsilon_{xx}^{0(i)} \\ \varepsilon_{yy}^{0(i)} \\ \varepsilon_{xy}^{0(i)} \end{Bmatrix} = \varepsilon_l^{(i)} + \varepsilon_{nl}^{(i)}$$

being

$$\varepsilon_l^{(i)} = \begin{Bmatrix} \dfrac{\partial u_0^{(i)}}{\partial x} \\ \dfrac{\partial v_0^{(i)}}{\partial y} \\ \dfrac{\partial u_0^{(i)}}{\partial y} + \dfrac{\partial v_0^{(i)}}{\partial x} \end{Bmatrix},$$

$$\varepsilon_{nl}^{(i)} = \begin{Bmatrix} \dfrac{1}{2}\left(\dfrac{\partial w_0^{(i)}}{\partial x}\right)^2 \\ \dfrac{1}{2}\left(\dfrac{\partial w_0^{(i)}}{\partial y}\right)^2 \\ \dfrac{\partial w_0^{(i)}}{\partial x}\dfrac{\partial w_0^{(i)}}{\partial y} \end{Bmatrix}, \tag{12}$$

$$\psi^{(i)} = \begin{Bmatrix} \dfrac{\partial \varphi_x^{(i)}}{\partial x} \\ \dfrac{\partial \varphi_y^{(i)}}{\partial y} \\ \dfrac{\partial \varphi_x^{(i)}}{\partial y} + \dfrac{\partial \varphi_y^{(i)}}{\partial x} \end{Bmatrix}$$

where $\varepsilon_l^{(i)}$, $\varepsilon_{nl}^{(i)}$, $\psi^{(i)}$ and $\varepsilon_s^{(i)}$ are linear, nonlinear, curvature and shear strains vectors, respectively, and keep in mind, calculating these equations are done by considering Eq. (4). Stress-strain relationship for each plate at any point can be written as below, if the plates assumed to be in conditions of plane stress.

$$\sigma^{(i)} = \begin{Bmatrix} \sigma_{xx}^{(i)} \\ \sigma_{yy}^{(i)} \\ \tau_{xy}^{(i)} \end{Bmatrix} = \bar{Q}\varepsilon^{(i)} = \begin{bmatrix} \bar{Q}_{11} & \bar{Q}_{12} & \bar{Q}_{16} \\ \bar{Q}_{12} & \bar{Q}_{22} & \bar{Q}_{26} \\ \bar{Q}_{16} & \bar{Q}_{26} & \bar{Q}_{66} \end{bmatrix} \begin{Bmatrix} \varepsilon_{xx}^{(i)} \\ \varepsilon_{yy}^{(i)} \\ \varepsilon_{xy}^{(i)} \end{Bmatrix}$$

$$\sigma_s^{(i)} = \bar{Q}_s\varepsilon_s^{(i)} = \begin{bmatrix} \bar{Q}_{44} & \bar{Q}_{45} \\ \bar{Q}_{45} & \bar{Q}_{55} \end{bmatrix} \begin{bmatrix} \varphi_y^{(i)} + \dfrac{\partial w_0^{(i)}}{\partial y} \\ \varphi_x^{(i)} + \dfrac{\partial w_0^{(i)}}{\partial x} \end{bmatrix} \tag{13}$$

where $\bar{Q}_{ij}(i,j = 1,2,6)$ are transformed reduced stiffness coefficients and $\bar{Q}_s$ is transformed shear stiffness matrix. Stiffness matrices for each plate can be calculated as

$$\left(E_{1_{ij}}, E_{2_{ij}}, E_{3_{ij}}\right) = \int_{-\frac{h}{2}}^{\frac{h}{2}} \bar{Q}_{ij}\,(1, z, z^2)dz, \quad i,j = 1,2,6$$
$$E_{1s_{ij}} = \int_{-\frac{h}{2}}^{\frac{h}{2}} \bar{Q}_{ij}\,dz, \quad i,j = 4,5 \tag{14}$$

In which, E_1, E_2, E_3 and E_{1s} are respectively extensional stiffness matrix, extensional-bending stiffness matrix, bending stiffness matrix and transverse shear stiffness matrix, where in the case of simple power law variations, they can be calculated as

$$E_1 = \left(E_m h + \frac{E_{cm}h}{n+1}\right)\begin{bmatrix} 1 & \upsilon & 0 \\ \upsilon & 1 & 0 \\ 0 & 0 & \dfrac{1-\upsilon}{2} \end{bmatrix}\left(\frac{1}{1-\upsilon^2}\right)$$

$$E_2 = \left(E_{cm}h^2\left(\frac{1}{n+2} + \frac{1}{2(n+1)}\right)\right)\begin{bmatrix} 1 & \upsilon & 0 \\ \upsilon & 1 & 0 \\ 0 & 0 & \dfrac{1-\upsilon}{2} \end{bmatrix}\left(\frac{1}{1-\upsilon^2}\right)$$

$$E_3 = \left(\frac{E_m h^3}{12} + E_{cm}h^3\left(\frac{1}{n+3} - \frac{1}{n+2} + \frac{1}{4(n+1)}\right)\right)\begin{bmatrix} 1 & \upsilon & 0 \\ \upsilon & 1 & 0 \\ 0 & 0 & \dfrac{1-\upsilon}{2} \end{bmatrix}\left(\frac{1}{1-\upsilon^2}\right) \tag{15}$$

$$E_{1s} = \left(E_m h + \frac{E_{cm}h}{n+1}\right) I_2 \left(\frac{1}{2(1+\upsilon)}\right)$$

where $E_{cm} = E_c - E_m$ and n is called volume fraction index which indicates the material variation profile through the thickness direction, and is non-negative real value and I is identity matrix. With the above definitions, the total potential energy of each plate-element can be divided into three parts, the first part, $U_m^{(i)}$, is strain energy associated with the in-plane stresses, the second part, $U_s^{(i)}$, is shear strain energy and the last part, $V_F^{(i)}$, is potential energy of the external forces.

$$\Pi^{(i)} = U_m^{(i)} + U_s^{(i)} + V_F^{(i)} \tag{16}$$

In which, the strain energy and the shear strain energy can be calculated as

$$\begin{aligned} U_m^{(i)} &= \frac{1}{2}\int_{V^{(i)}} \varepsilon^{(i)^T}\sigma^{(i)}dV^{(i)} \\ &= \frac{1}{2}\int_{\Omega^{(i)}}\int_{-\frac{h}{2}}^{\frac{h}{2}} \varepsilon^{(i)^T}\bar{Q}\varepsilon^{(i)}dz d\Omega^{(i)} \\ &= \int_{\Omega^{(i)}}\left(\frac{1}{2}\varepsilon_l^{(i)^T}E_1\varepsilon_l^{(i)} + \varepsilon_l^{(i)^T}E_2\psi^{(i)} + \frac{1}{2}\psi^{(i)^T}E_3\psi^{(i)}\right)d\Omega^{(i)} \\ &+ \int_{\Omega^{(i)}}\left(\varepsilon_l^{(i)^T}E_1\varepsilon_{nl}^{(i)} + \varepsilon_{nl}^{(i)^T}E_2\psi^{(i)}\right)d\Omega^{(i)} \\ &+ \int_{\Omega^{(i)}}\frac{1}{2}\varepsilon_{nl}^{(i)^T}E_1\varepsilon_{nl}^{(i)}d\Omega^{(i)} \end{aligned} \tag{17a}$$

$$\begin{aligned} U_s^{(i)} &= \frac{1}{2}k_s\int_{V^{(i)}} \varepsilon_s^{(i)^T}\sigma_s{}^{(i)}dV^{(i)} \\ &= \frac{1}{2}k_s\int_{\Omega^{(i)}}\int_{-\frac{h}{2}}^{\frac{h}{2}} \varepsilon_s^{(i)^T}\bar{Q}_s\varepsilon_s^{(i)}dz d\Omega^{(i)} \\ &= \frac{1}{2}k_s\int_{\Omega^{(i)}} \varepsilon_s^{(i)^T}E_{1s}\varepsilon_s^{(i)}d\Omega^{(i)} \end{aligned} \tag{17b}$$

where k_s is shear correction factor and assumed to be 5/6 in this study. According to transformation technique mentioned before, the integrals in these equations should be transformed as well. For instance, the transformation of an integral of a typical function $f(x,y)$ in two-dimensional domain Ω is performed as follows

$$\begin{aligned} &\int_{\Omega} f(x,y)\ d\Omega \\ &= \int_{-1}^{1}\int_{-1}^{1} f\big(X(\xi,\eta), Y(\xi,\eta)\big)\left|\frac{\partial(X,Y)}{\partial(\xi,\eta)}\right| d\xi\, d\eta \end{aligned} \tag{18}$$

Calculating the values of potential energy of external forces depends on how the in-plane compressive load is applied to the perforated functionally graded plate. In accordance with Figs. 1 and 2, the potential energy of external forces for each plate-element can be calculated as

$$V_F^{(i)} = \begin{cases} \dfrac{W_e^{(i)}}{l}N_x\,\delta_c^{\tau^{(i)}}\Big|_{x=-L_e^{(i)}/2} & i = 1,3,5 \\ -\dfrac{W_e^{(i)}}{l}N_x\,\delta_c^{\tau^{(i)}}\Big|_{x=L_e^{(i)}/2} & i = 2,4,6 \end{cases} \tag{19}$$

It is again emphasized that in this paper the plate is only subjected to in-plane compressive load N_x. As it can be observed, in Eq. (17(a)) the strain energy, $U_m^{(i)}$, is divided into three parts which are quadratic, cubic and quartic functions of the unknowns, respectively. By using Eqs. (7), (17) and (19), the total potential energy equation can be finally obtained as

$$\Pi = \sum_{i=1}^{6}\left(U_m^{(i)} + U_s^{(i)} + V_F^{(i)}\right) + P \tag{20}$$

The only point that needs to be raised here is how to calculate the integrations in the total potential energy equation. Since integrating analytically is very timely and almost impossible, so in the current study, the domain is discretized by a set of nodes and therefore the transformed continuous integrals should be replaced by summations where they can be calculated over all nodes. To do that, for elements number 1, 2, 5 and 6, Legendre-Gauss-Lobatto nodes are considered here and their coordinates are obtained by solving the following

$$\begin{cases} P'_{m-1}(\xi_i) = 0 \\ P'_{n-1}(\eta_j) = 0 \end{cases} \tag{21}$$

where the parameters m and n denote the number of nodes in ξ and η directions, respectively and ξ_i and η_j are non-dimensional coordinates of i^{th} and j^{th}node in the ξ and η directions. In order to achieve better accuracy and also to avoid excessive number of nodes to reduce computational costs, an appropriate weight coefficient should be considered for each node. Calculation of the weight coefficients for nodes is performed by taking idea from Gauss- Lobatto rules. Therefore, the typical continuous integral in Eq. (18) can be rewritten as

$$\begin{aligned} &\int_\Omega f(x,y)\ d\Omega \\ &= \int_{-1}^{1}\int_{-1}^{1} \underbrace{f\big(X(\xi,\eta),Y(\xi,\eta)\big)\left|\frac{\partial(X,Y)}{\partial(\xi,\eta)}\right|}_{g(\xi,\eta)}\ d\xi\ d\eta \\ &= \sum_{j=1}^{n}\sum_{i=1}^{m} \varpi_i \omega_j g\big(\xi_i,\eta_j\big) \end{aligned} \tag{22}$$

where i and j refer to the i^{th} node along ξ-direction and j^{th} node along η-direction and the coefficients ϖ_i and ω_j are weight coefficients of nodes along ξ and η-directions, respectively and they can be computed by

$$\varpi_i = \frac{2}{m(m-1)[P_{m-1}(\xi_i)]^2} \tag{23a}$$

$$\omega_j = \frac{2}{n(n-1)[P_{n-1}(\eta_i)]^2} \tag{23b}$$

It should be noted that in the case of elements 3 and 4, the integrals are taken by applying the double exponential technique, known as Tanh-sinh quadrature, due to the presence of singularities at both ends of the integrals. Tanh-sinh quadrature is less efficient than Gaussian quadrature for smooth integrands, however unlike the Gaussian quadrature, it has the ability to apply onto integrands that have singularities or infinite derivatives at one or both endpoints of the integration interval. These integrals for elements 3 and 4 can be calculated as shown in Eq. (24).

$$\begin{aligned} &\int_\Omega f(x,y)\ d\Omega \\ &= \int_{-1}^{1}\int_{-1}^{1} f\big(X(\xi,\eta),Y(\xi,\eta)\big)\left|\frac{\partial(X,Y)}{\partial(\xi,\eta)}\right|\ d\xi\ d\eta \\ &= \int_{-1}^{1}\int_{-1}^{1} g(\xi,\eta)\ d\xi\ d\eta \\ &= \int_{-t_a}^{t_a}\int_{-s_a}^{s_a} \underbrace{g\big(\xi(s),\eta(t)\big)\xi'(s)\ \eta'(t)}_{h(\xi,\eta)}\ ds\ dt \\ &= \sum_{j=1}^{n}\sum_{i=1}^{m} \rho_i \rho_j h\big(\xi_i,\eta_j\big) \end{aligned} \tag{24}$$

being

$$\xi_i = \tanh\left(\frac{\pi}{2}\sinh(s_i)\right), s_i = -s_a + (i-1)\ell_\xi \tag{25a}$$

$$\eta_j = \tanh\left(\frac{\pi}{2}\sinh(t_j)\right), t_j = -t_a + (j-1)\ell_\eta \tag{25b}$$

$$\rho_i = \frac{\frac{\pi}{2}\cosh(s_i)}{\cosh^2\left(\frac{\pi}{2}\sinh(s_i)\right)}\ell_\xi, \qquad \ell_\xi = \frac{2s_a}{m-1} \tag{25c}$$

$$\rho_j = \frac{\frac{\pi}{2}\cosh(t_i)}{\cosh^2\left(\frac{\pi}{2}\sinh(t_i)\right)}\ell_\eta, \qquad \ell_\eta = \frac{2t_a}{n-1} \tag{25d}$$

where the coefficients ρ_i and ρ_j are weight coefficients of the nodes in ξ and η-directions. The value of s_a and t_a are taken experimentally and in this paper, they are chosen to be equal to $2\pi/3$. The elements number 1, 2, 5 and 6 are discretized by 13 nodes along each direction and elements 3 and 4 by 25×25 nodes.

The solution of the nonlinear problem is sought through the application of the principle of minimum potential energy. Also, to obtain the solution of the nonlinear algebraic equations, the well-known quadratic extrapolation technique is used. The details of the steps for solving the nonlinear equations using quadratic extrapolation technique have been described in the study done by Mehrparvar and Ghannadpour (2018).

3. Numerical results and discussion

The formulation presented in this research has been precisely implemented in the Fortran 77 programming software package. Parallel programming technique has been

used in this computer program to reduce the execution time on multicore processors. This program is executed on a computer with TYAN FT48-B8812 mainboard, 4 AMD CPU by 2.20 GHz frequency (4×16 cores) and 128.00 GB RAM. Using this program, the post-buckling and nonlinear results for some FGPs are obtained and presented in this section. The FGPs considered here consist of aluminum (Al) and zirconia (ZrO_2) components with material properties taken from research done by Mehrparvar and Ghannadpour (2018). The calculated results for moderately thick perforated FGPs using the developed computer program in this research have been compared by those obtained by ABAQUS commercial software, in which, a FGP is meshed with 2500 S4R shell elements. As represented in Table 1, three different boundary conditions are considered in this study in which the plates are subjected to in-plane compressive load N_x normal to the vertical edges $x = \pm l/2$.

In addition to verifying the nonlinear results with ABAQUS software, the results for buckling behavior of some simply-supported isotropic plates with circular cutout are compared with those presented by Ritche and Rhodes (1975) and those obtained by ABAQUS in Table 2. The non-dimensional values for buckling coefficient in this table have been computed based on the ratio of buckling load of the perforated plate to that of the perfect plate.

To do convergence studies for obtaining the sufficient number of terms (N_t) in the displacement fields, the square FGPs with linear variations of material properties along the thickness, i.e. $n = 1$ are assumed having horizontal elliptical cutout with $a = 0.5l$ and $b = 0.3l$. These FGPs are also considered to have CSCS boundary conditions as shown in Fig. 2. The post-buckling behavior of these plates for different number of terms is depicted in Fig. 6 as non-dimensional form of load-deflection. Non-dimensional load P is defined as $N_x l^2/E_m h^3$ where E_m refers to Young's modulus of the metal component and non-dimensional deflection W is w/h. As shown in this figure, if there are 6×6 terms in each displacement field and for each plate-element, the results will converge and will fit on the finite element results.

Fig. 7 shows the effect of volume fraction index, which displayed n (see Eq. (15)), on post-buckling and nonlinear behavior of square plate with elliptical cutout, in which the cutout sizes are $a = 0.2l$ and $b = 0.5l$.

Table 2 Non-dimensional buckling values for some perforated isotropic plate with circular cutout ($l = 1\ m\ , h = 0.001m, E = 7.06 \times 10^{11}\ N/m^2\ , \nu = 0.3$)

d/l	present	Ritche and Rhodes (1975)	ABAQUS
0.2	0.90	0.92	0.89
0.4	0.79	0.76	0.77
0.6	0.73	0.64	0.72

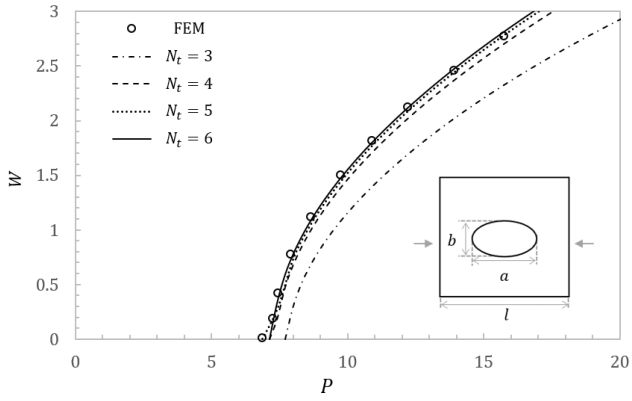

Fig. 6 Convergence study for FGP $(n = 1)$ containing elliptical cutout, $a = 0.5l$ and $b = 0.3l$, with CSCS boundary conditions

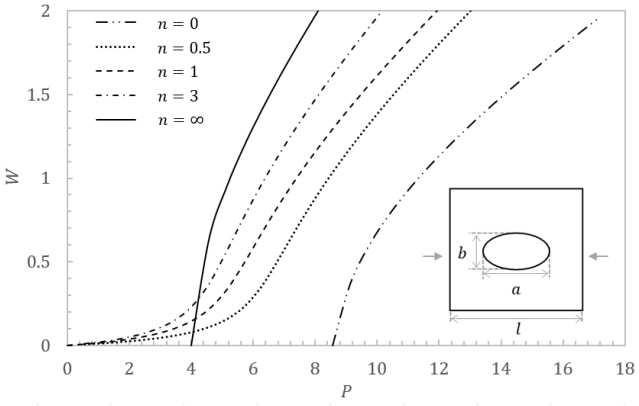

Fig. 7 Effect of volume fraction index on nonlinear behavior of FGP containing elliptical cutout, $a = 0.2l$ and $b = 0.5l$, with SSSS boundary conditions

All edges of the plates are assumed to be simply-supported. The maximum deflections of the considered plates for $n = 0\ , 0.5\ , 1\ , 3\ , \infty$ have been shown in this figure. As shown in Figs. 6 and 7, for FG plates with $n = 0$, there are two completely different behaviors. In the results of Fig. 6, some edges of the plate were clamped and therefore, in its behavior, the bifurcation state is observed. Therefore, it has buckling, while for simply-supported FG plates, buckling behavior is not observed and the plates bend as they are loaded.

The proposed formulation in this study is capable of modeling circular holes. To illustrate this capability, non-linear behaviors of square FG plates can be found in Figs. 8 to 10, with circular holes of different sizes. As it can be seen, the results have been presented for some selected values of $0.1\ , 0.2\ , 0.3\ , 0.4$ and 0.5 for ratio of cutout diameter to plate length. The non-dimensional form of load-deflection behavior for SSSS FG plates have been displayed in Fig. 8 and similar results have been presented for CSCS ceramic plates in Fig. 9. The non-dimensional form of the results for variations of load versus in-plane displacement

($\delta_c^u = u/h$) for CSCS ceramic plates is also depicted in Fig. 10.

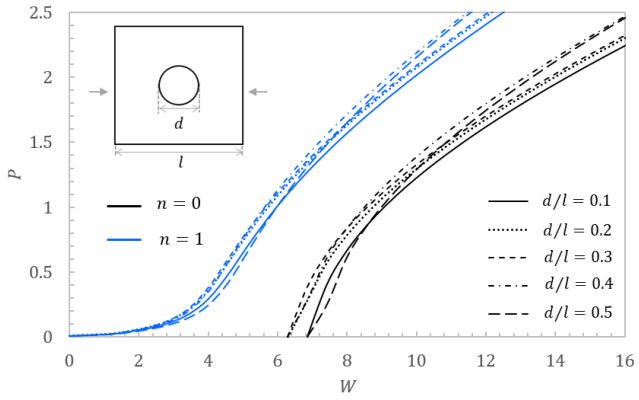

Fig. 8 Effects of circular cutout size on maximum deflection of FGP with SSSS boundary conditions and $n = 0$ & 1

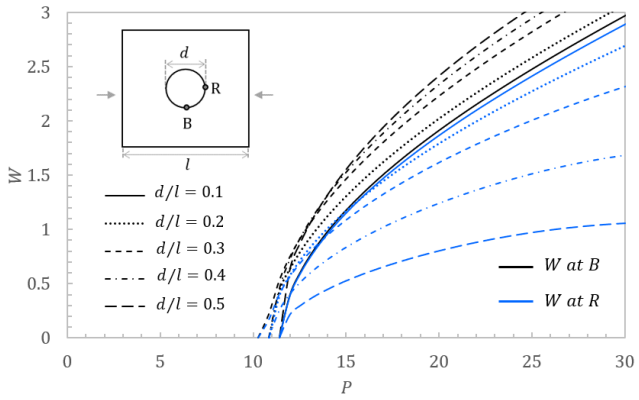

Fig. 9 Effects of circular cutout size on nonlinear behavior of ceramic plate with CSCS boundary conditions

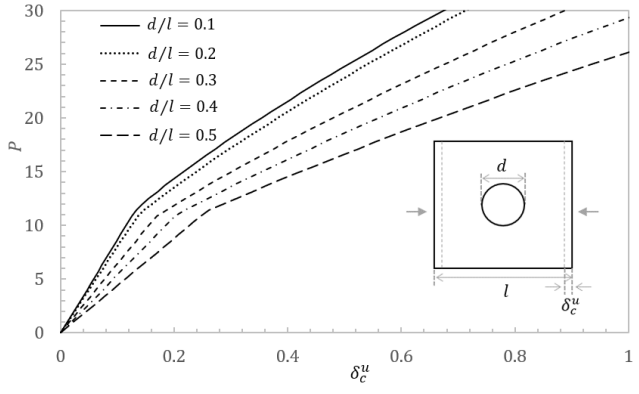

Fig. 10 Effects of circular cutout size on post-buckling stiffness of ceramic plate with CSCS boundary conditions

As it is seen, by increasing the cutout size, the buckling load decreases slightly. However, in ratios 0.4 and 0.5, this amount again increases. As expected and according to the results presented in these figures, the post-buckling behavior is completely affected by the boundary conditions, and when the out-of-plane boundary conditions are changed from SSSS to CSCS, the nonlinear behavior is completely changed. It could be observed in Fig. 10 that by increasing the cutout size in ceramic plates, the post-buckling stiffness of the plates significantly decreases.

One of the important features of the method introduced in this study is the possibility of modeling of elliptical holes with different sizes. Also, in the case of elliptical shaped cutout, the position of the elliptical hole with respect to the load direction is also an important parameter that plays an effective role in the design of perforated structures. In Figs. 11 and 12, the post-buckling responses of ceramic plates with SSSS boundary conditions for plate containing vertical and horizontal elliptical cutout have been presented. Various sizes of elliptical cutout are studied as well as perfect plate. As it can be observed, in the case of horizontal cutouts the buckling load of the plates is lower than the perfect plate and this value increases by increasing the cutout size. Similar behavior could be observed for post-buckling response. However, in the case of vertical cutout, the buckling load of the plates are significantly greater than the perfect plate although by increasing the cutout size the buckling load decreases. By observing the Fig. 11, it's worth mentioning that the post-buckling stiffnesses of the plates in these two states are very close to each other, although the amount of buckling load and the pre-buckling stiffnesses are quite different.

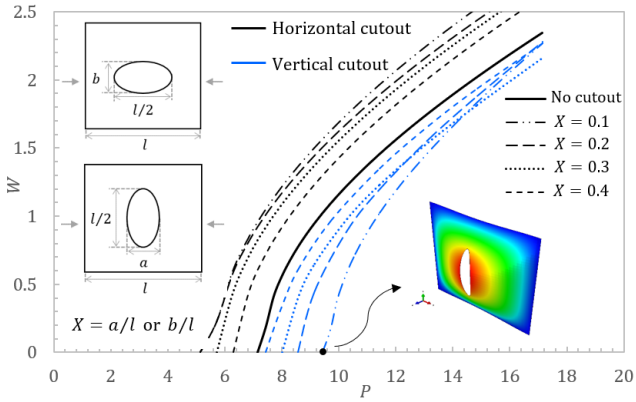

Fig. 11 Effects of elliptical cutout size on maximum deflection of ceramic plates with SSSS boundary conditions

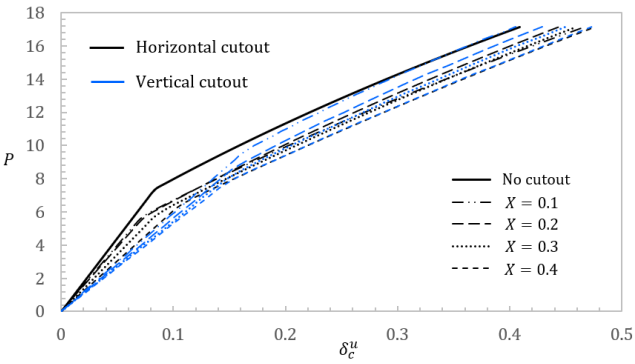

Fig. 12 Effects of elliptical cutout size on pre- and post-

buckling of ceramic plates with SSSS boundary conditions.

Similar to the results of perforated plates with SSSS boundary conditions, the results correspond to the FG plates ($n = 1$) containing horizontal and vertical cutouts for both CSCS and CCCS boundary conditions have been depicted in Figs. 13 to 16. As it can be seen the same outcome is obtained for vertical cutouts though, in the case of horizontal cutouts, very similar results are obtained for buckling loads and post-buckling responses that are mostly independent of the size of ellipse, and this can be due to the application of clamped boundary conditions that have had very little effects on the presence of the hole.

According to the previous results, it was found that the position of the ellipse relative to the loading direction has significant effects on the results. Therefore, taking into account the angles between these two situations may also result in interesting results. On the other hand, one of the capabilities of the formulation developed in this study is the possibility of modeling this geometry. To examine these conditions, an angle α is defined for the ellipse rotation which is the angle between y-axis and ellipse's semi-major axis.

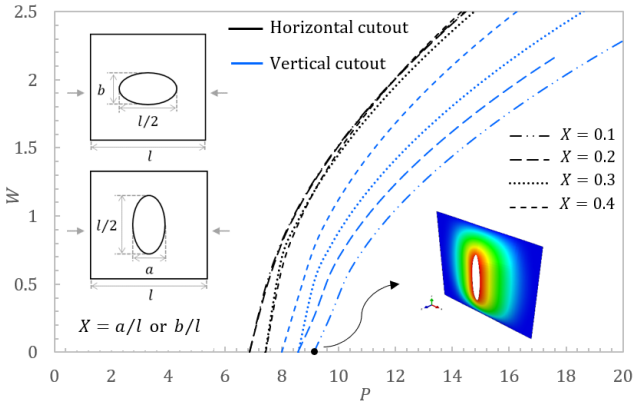

Fig. 13 Effects of elliptical cutout size on maximum deflection of FGPs with CSCS boundary conditions and $n = 1$

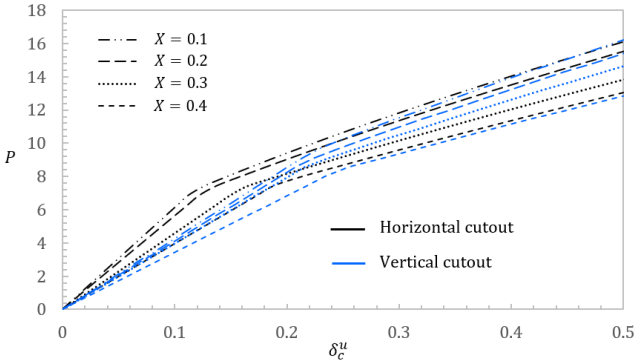

Fig. 14 Effects of elliptical cutout size on post-buckling stiffness of FGP with CSCS boundary conditions and $n = 1$

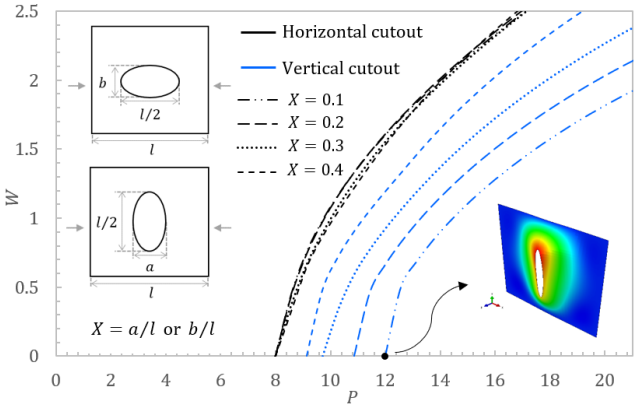

Fig. 15 Effect of elliptical cutout size on maximum deflection of FGP with CCCS boundary conditions and $n = 1$

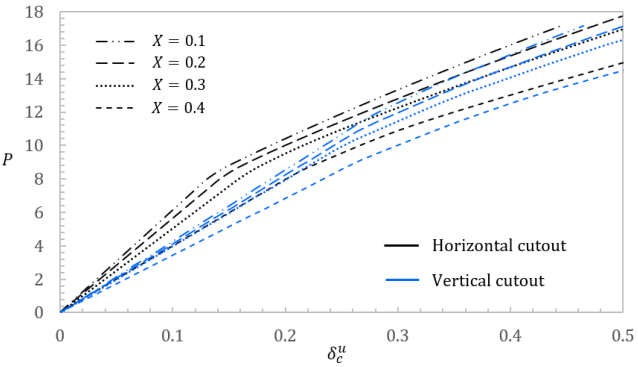

Fig. 16 Effects of elliptical cutout size on post-buckling of FGP with CCCS boundary conditions and $n = 1$

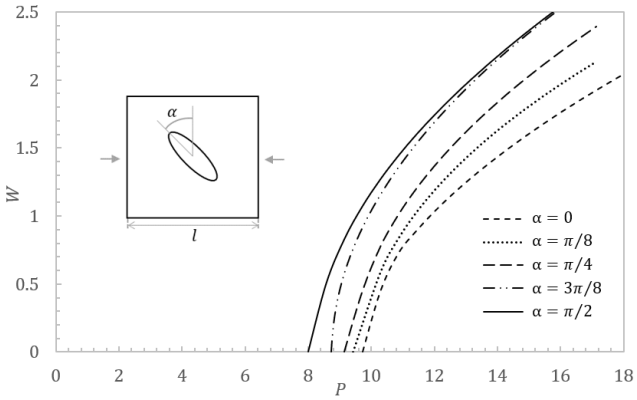

Fig. 17 Post-buckling response of CSCS FG plates containing oblique elliptical cutouts with $a = 0.1l$ and $b = 0.5l$

The post-buckling results for some square FGPs ($n = 1$) containing oblique elliptical hole and with CSCS boundary conditions are presented in Fig. 17. As it can be seen, the results have been obtained for $\alpha = 0^{\circ}, \pi/8, \pi/4, 3\pi/8$ and $\pi/2$ and for an ellipse with dimensions $a = 0.1l$ and $b = 0.5l$. It is observed that by rotating the ellipse from vertical to horizontal, the buckling load decreases.

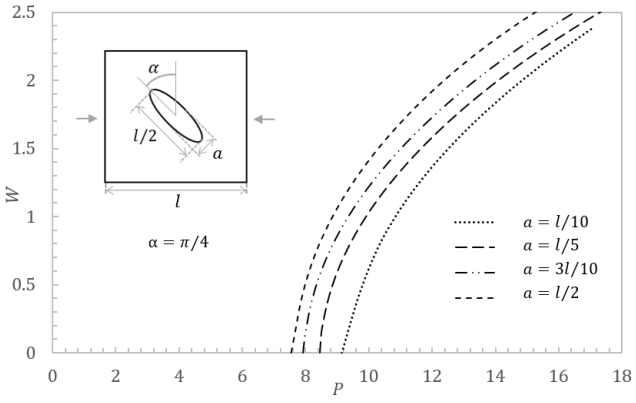

Fig. 18 Post-buckling response of CSCS FG plates containing elliptical cutout $\alpha = \pi/4$ with different aspect ratios

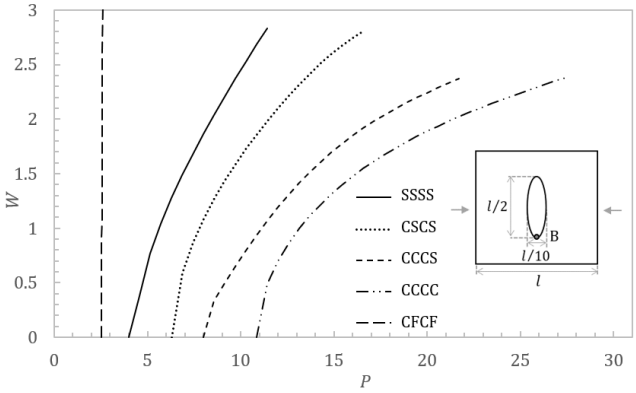

Fig. 19 Effects of different boundary conditions on out-of-plane deflection of point B located at the bottom of elliptic cutout in a metal plate

Fig. 18 represents the effects of different aspect ratios of elliptical cutouts on post-buckling behavior of functionally graded plates in which the material properties are chosen to vary linearly with respect to the thickness. In this figure, the results are for perforated plates in which the angle between y-axis and cutout's semi-major axis is chosen to be $\pi/4$ and $a = l/10, l/5, 3l/10$ and $l/2$. Increasing the ellipse aspect ratio has increased the buckling load.

In addition to previous studies, another investigation can be made for load-deflection behavior of metal plates containing the elliptical cutout when the boundary conditions of the plates are changed. (see Fig. 19). The cutout size is assumed to be $a = 0.1l$ and $b = 0.5l$. In addition to the previously mentioned boundary conditions, two other sets of boundary conditions are also studied in this figure. The first set is corresponding to the perforated plate with all clamped edges (CCCC) and the second one (CFCF) is for a metal plate with two free unloaded edges (i.e. edges No. 2 and 4) and two clamped loaded ends (i.e. edges No. 1 and 3). As expected, the CCCC perforated plate has higher buckling load with respect to all other conditions and the plate with two free unloaded edges behaves as a wide column and therefore it has Euler buckling.

7. Conclusions

A new computational procedure was introduced in the current study to model the oblique elliptical cutouts. By the technique introduced, the post-buckling and nonlinear behaviors of functionally graded plates containing elliptical hole were examined when they were subjected to in-plane compressive loads. The governing equations were obtained based on the FSDT and Von-Karman nonlinearity assumptions. The displacement fields of the problems were approximated based on the Ritz method and by Legendre polynomials. The plates were assembled by six plate-elements which were connected by applying the penalty method and thus the total potential energy of the plates was the summation of potential energy of the elements. To obtain the nonlinear equilibrium equations the principle of minimum potential energy was used and to solve these nonlinear algebraic equations the quadratic extrapolation technique was employed to calculate the degrees of freedom in the displacement fields. The results were presented in non-dimensional graphical forms and for FG plates with different boundary conditions, cutout size, orientation and shape. In the results it was seen that the buckling load and post-buckling response of the FG plates are considerably affected by the shape of the cutouts and particularly their orientation. For instance, the FG plate with elliptical cutout perpendicular to the loading direction has higher buckling load with respect to the case in which the plate has elliptical cutout aligned along the loading direction. It is also worth mentioning that in this paper, for the first time, a new semi-analytical method was introduced that can model the holes with curved boundaries and were used in nonlinear and post-buckling analyzes. Finally, the proposed method, with the lowest computations, with lowest number of degrees of freedom and with high accuracy is capable to find nonlinear responses of FG plates and can be extended to other types of structures.

References

Alinia, M.M. and Ghanndpour, S.A.M. (2009), "Nonlinear analysis of pressure loaded FGM plates", *Compos. Struct.*, **88**(3), 354-359. https://doi.org/10.1016/j.compstruct.2008.04.013.

Baba, B.O. and Baltaci, A. (2007), "Buckling characteristics of symmetrically and antisymmetrically laminated composite plates with central cutout", *Appl. Compos. Mater.*, **14**, 265-276. https://doi.org/10.1007/s10443-007-9045-z.

Bailey, R. and Wood, J. (1996), "Stability characteristics of composite panels with various cutout geometries", *Compos. Struct.*, **35**(1), 21-31. https://doi.org/10.1016/0263-8223(96)00021-9.

Britt, V.O. (1994), "Shear and compression buckling analysis for anisotropic panels with elliptical cutouts", *AIAA J.*, **32**(11) 2293-2299. https://doi.org/10.2514/3.12289.

Chen, Y., Jin, G. and Liu, Z. (2014), "Flexural and in-plane vibration analysis of elastically restrained thin rectangular plate with cutout using Chebyshev–Lagrangian method", *Int. J. Mech. Sci.*, **89**, 264-278. https://doi.org/10.1016/j.ijmecsci.2014.09.006.

Cheng, B. and Li, C. (2012), "Buckling behavior of strengthened

perforated plates under shear loading", *Steel Compos. Struct.*, **13**(4), 367-382. https://doi.org/10.12989/scs.2012.13.4.367.

Choudhary, P.K. and Jana, P. (2018), "Position optimization of circular/elliptical cutout within an orthotropic rectangular plate for maximum buckling load", *Steel Compos. Struct.*, **29**(1), 39-51. https://doi.org/10.12989/scs.2018.29.1.39.

Ghannadpour, S.A.M. and Alinia, M.M. (2006), "Large deflection behavior of functionally graded plates under pressure loads", *Compos. Struct.*, **75**(1-4), 67-71. https://doi.org/10.1016/j.compstruct.2006.04.004.

Ghannadpour, S.A.M. and Karimi, M. (2018), "Domain decomposition technique to simulate crack in nonlinear analysis of initially imperfect laminates", *Struct. Eng. Mech.*, **68**(5), 603-619. https://doi.org/10.12989/sem.2018.68.5.603.

Ghannadpour, S.A.M. and Kiani, P. (2018), "Nonlinear spectral collocation analysis of imperfect functionally graded plates under end-shortening", *Struct. Eng. Mech.*, **66**(5), 557-568. https://doi.org/10.12989/sem.2018.66.5.557.

Ghannadpour, S.A.M. and Mehrparvar, M. (2018), "Energy effect removal technique to model circular/elliptical holes in relatively thick composite plates under in-plane compressive load", *Compos. Struct.*, **202**, 1032-1041. https://doi.org/10.1016/j.compstruct.2018.05.026.

Ghannadpour, S.A.M. and Shakeri, M. (2018), "Energy based collocation method to predict progressive damage behavior of imperfect composite plates under compression", *Latin Am. J. Solids Struct.*, **15**(4).

Ghannadpour, S.A.M., Karimi, M. and Tornabene, F. (2019), "Application of plate decomposition technique in nonlinear and post-buckling analysis of functionally graded plates containing crack", *Compos. Struct.*, **220**, 158-167. https://doi.org/10.1016/j.compstruct.2019.03.025.

Ghannadpour, S.A.M., Najafi, A. and Mohammadi, B. (2006), "On the buckling behavior of cross-ply laminated composite plates due to circular/elliptical cutouts", *Compos. Struct.*, **75**, 3-6. https://doi.org/10.1016/j.compstruct.2006.04.071.

Ghannadpour, S.A.M., Ovesy, H.R. and Nassirnia, M. (2012), "An investigation on buckling behavior of functionally graded plates using finite strip method", *Appl. Mech. Mater.*, **152-154**, 1470-1476. https://doi.org/10.4028/www.scientific.net/AMM.152-154.1470.

Heidari-Rarani, M. and Kharratzadeh, M. (2019), "Buckling behavior of composite cylindrical shells with cutout considering geometric imperfection", *Steel Compos. Struct.*, **30**(4), 305-313. https://doi.org/10.12989/scs.2019.30.4.305.

Jain, P. and Kumar, A. (2004), "Postbuckling response of square laminates with a central circular/elliptical cutout", *Compos. Struct.*, **65**(2), 179-185. https://doi.org/10.1016/j.compstruct.2003.10.014.

Javaheri, R. and Eslami, M.R. (2002), "Buckling of functionally graded plates under in-plane compressive load", *J. Appl.Math. Mech.*, **82**(4), 277-283. https://doi.org/10.1002/1521-4001(200204)82:4<277::AID-ZAMM277>3.0.CO;2-Y.

Kandasamya, R., Dimitrib, R. and Tornabene, F. (2016), "Numerical study on the free vibration a nd thermal buckling behavior of moderately thick functionally graded structures in thermal environment", *Compos. Struct.*, **157**, 207-221. https://doi.org/10.1016/j.compstruct.2016.08.037.

Kar, V.R. and Panda S.K., (2016), "Post-buckling behavior of shear deformable functionally graded curved shell panel under edge compression", *Int. J. Mech. Sci.*, **115-116**, 318-324. https://doi.org/10.1016/j.ijmecsci.2016.07.014.

Koizumi, M. (1997), "FGM activities in Japan", *Compos. Part B*, **28**(1-2), 1-4. https://doi.org/10.1016/S1359-8368(96)00016-9.

Komur, M.A. and Sonmez, M. (2008), "Elastic buckling of rectangular plates under linearly varying in-plane normal load with a circular cutout", *Mech. Res. Commun.*, **35**(6), 361-371. https://doi.org/10.1016/j.mechrescom.2008.01.005.

Komur, M.A., Sen, F., Ataș, A. and Arslan, N. (2010), "Buckling analysis of laminated composite plates with an elliptical/circular cutout using FEM", *Adv. Eng. Softw.*, **41**(2), 161-164. https://doi.org/10.1016/j.advengsoft.2009.09.005.

Kong, C.W., Hong, C.S. and Kim, C.G. (2001), "Postbuckling strength of composite plate with a hole", *J. Reinforced Plastics Compos.*, **20**(6), 466-481. https://doi.org/10.1177/073168401772678652.

Kopriva, D.A. (2009), Implementing spectral methods for partial differential equations: Algorithms for scientists and engineers, Springer Science & Business Media.

Kumar, D. and Singh, S.B. (2010), "Effect of boundary conditions on buckling and postbuckling responses of composite laminate with various shaped cutouts", *Compos. Struct.*, **92**(3), 769-779. https://doi.org/10.1016/j.compstruct.2009.08.049.

Kumar, D. and Singh, S.B. (2010), "Postbuckling strengths of composite laminate with various shaped cutouts under in-plane shear", *Compos. Struct.*, **92**(12), 2966-2978. https://doi.org/10.1016/j.compstruct.2010.05.008.

Lee, Y.Y., Zhao, X. and Reddy, J.N. (2010), "Postbuckling analysis of functionally graded plates subject to compressive and thermal loads", *Computer. Method. Appl. M.*, **199**(25-28), 1645-1653. https://doi.org/10.1016/j.cma.2010.01.008.

Ma, L.S. and Wang, T.J. (2003), "Nonlinear bending and post-buckling of a functionally graded circular plate under mechanical and thermal loadings", *Int. J. Solids Struct.*, **40**(13-14), 3311-3330. https://doi.org/10.1016/S0020-7683(03)00118-5.

Ma, Y., Cheng, X., Wang, Z., Guo, X., Zhang, J. and Xu, Y. (2018), "Buckling and post-buckling behaviors of 1/3 composite cylindrical shell with an opening", *Steel Compos. Struct.*, **27**(5), 555-566. https://doi.org/10.12989/scs.2018.27.5.555.

Mehrparvar, M. and Ghannadpour, S.A.M. (2018), "Plate assembly technique for nonlinear analysis of relatively thick functionally graded plates containing rectangular holes subjected to in-plane compressive load", *Compos. Struct.*, **202**, 867-880. https://doi.org/10.1016/j.compstruct.2018.04.053.

Mohammadi, B., Najafi, A. and Ghannadpour, S.A.M. (2006), "Effective widths of compression-loaded of perforated cross-ply laminated composites", *Compos. Struct.*, **75**(1-4), 7-13. https://doi.org/10.1016/j.compstruct.2006.04.025.

Nemeth, M.P. (1990), "Buckling and postbuckling behavior of square compression-loaded graphite-epoxy plates with circular cutouts", NASA Technical Paper 3007.

Noor, A.K. and Kim, Y.H. (1996), "Buckling and postbuckling of composite panels with cutouts subjected to combined edge shear and temperature change", *Compos. Struct.*, **60**(2), 203-222. https://doi.org/10.1016/0045-7949(95)00398-3.

Ovesy, H.R. and Ghannadpour, S.A.M. (2007), "Large deflection finite strip analysis of functionally graded plates under pressure loads", *Int. J. Struct. Stab. Dynam.*, **7**(2), 193-211. https://doi.org/10.1142/S0219455407002241.

Ovesy, H.R., Ghannadpour, S.A.M. and Nassirnia, M. (2015), "Post-buckling analysis of rectangular plates comprising functionally graded strips in thermal environment", *Compos. Struct.*, **147**, 209-215. https://doi.org/10.1016/j.compstruc.2014.09.011.

Pradhan, K.K. and Chakraverty, S. (2015), "Static analysis of functionally graded thin rectangular plates with various boundary supports", *Arch. Civil Mech. Eng.*, **15**(3), 721-734. https://doi.org/10.1016/j.acme.2014.09.008.

Rajanna, T., Banerjee, S., Desai, Y.M. and Prabhakara, D.L. (2016), "Vibration and buckling analyses of laminated panels with and without cutouts under compressive and tensile edge loads", *Steel Compos. Struct.*, **21**(1), 37-55. http://dx.doi.org/10.12989/scs.2016.21.1.037.

Reddy, J.N. (1982), "Large amplitude flexural vibration of layered composite plates with cutouts", *J. Sound Vib.*, **83**(1), 1-10. https://doi.org/10.1016/S0022-460X(82)80071-0.

Reddy, J.N. (2004), Mechanics of laminated composite plates and shells: theory and analysis, CRC Press, Boca Raton, U.S.A.

Ritchie, D. and Rhodes, J. (1975), "Buckling and postbuckling behaviour of plates with holes", *The Aeronautical Quarterly*, **26**(4), 281-296. https://doi.org/10.1017/S0001925900007435.

Sherafat, M.H., Ovesy, H.R. and Ghannadpour, S.A.M. (2013), "Buckling analysis of functionally graded plates under mechanical loading using higher order functionally graded strip", *Int. J. Struct. Stab. Dynam.*, **13**(6) 1350033. https://doi.org/10.1142/S0219455413500338.

Srivatsa, K.S. and Krishna Murty, A.V. (1992), "Stability of laminated composite plates with cut-outs", *Comput. Struct.*, **43**(2), 273-279. https://doi.org/10.1016/0045-7949(92)90144-O.

Taheri-Behrooz, F. and Omidi, M. (2018), "Buckling of axially compressed composite cylinders with geometric imperfections", *Steel Compos. Struct.*, **29**(4), 557-567. https://doi.org/10.12989/scs.2018.29.4.557.

Vandenbrink, D.J. and Kamat, M.P. (1987), "Post-buckling response of isotropic and laminated composite square plates with circular holes", *Finite Elem. Anal. Des.*, **3**(3), 165-174. https://doi.org/10.1016/0168-874X(87)90021-7.

Wu, Tsung-Lin, Shukla, K.K. and Huang, Jin H. (2007), "Post-buckling analysis of fuctionally graded rectangular plates", *Compos. Struct.*, **81**(1), 1-10. https://doi.org/10.1016/j.compstruct.2005.08.026.

Yang, J. and Shen, Hui-Shen (2003), "Non-linear analysis of functionally graded plates under transverse and in-plane loads", *Int. J. Non-Linear Mech.*, **38**(4), 467-482. https://doi.org/10.1016/S0020-7462(01)00070-1.

Yang, J., Liew, K.M. and Kitipornchai, S. (2006), "Imperfection sensitivity of the post-buckling behavior of higher-order shear deformable functionally graded plates", *Int. J. Solids Struct.*, **43**(17), 5247-5266. https://doi.org/10.1016/j.ijsolstr.2005.06.061.

CC